ACS OMEGA

Open Access

http://pubs.acs.org/journal/acsodf

Article

Study of PEG-*b*-PLA/Eudragit S100 Blends on the Nanoencapsulation of Indigo Carmine Dye and Application in Controlled Release

Shaked Ashkenazi,[‖] Pnina Matsanov,[‖] Eid Nassar-Marjiya, Shady Farah, and Iris S. Weitz*

Cite This: *ACS Omega* 2024, 9, 13382−13390

Read Online

ACCESS | Metrics & More | Article Recommendations | Supporting Information

ABSTRACT: A nanocapsule shell of poly(ethylene glycol)-*block*-poly(D,L-lactic acid) (PEG-*b*-PLA) mixed with anionic Eudragit S100 (90/10% w/w) was previously used to entrap and define the self-assembly of indigo carmine (IC) within the hydrophilic cavity core. In the present work, binary blends were prepared by solution mixing at different PEG-*b*-PLA/Eudragit S100 ratios (namely, 100/0, 90/10, 75/25, and 50/50% w/w) to elucidate the role of the capsule shell in tuning the encapsulation of the anionic dye (i.e., IC). The results showed that the higher content of Eudragit S100 in the blend decreases the miscibility of the two polymers due to weak intermolecular interactions between PEG-*b*-PLA and Eudragit S100. Moreover, with an increase in the amount of Eudragit S100, a higher thermal stability was observed related to the mobility restriction of PEG-*b*-PLA chains imposed by Eudragit S100. Formulations containing 10 and 25% Eudragit S100 exhibited an optimal interplay of properties between the negative surface charge and the miscibility of the polymer blend. Therefore, the anionic character of the encapsulating agent provides sufficient accumulation of IC molecules in the nanocapsule core, leading to dye aggregates following the self-assembly. At the same time, the blending of the two polymers tunes the IC release properties in the initial stage, achieving slow and controlled release. These findings give important insights into the rational design of polymeric nanosystems containing organic dyes for biomedical applications.

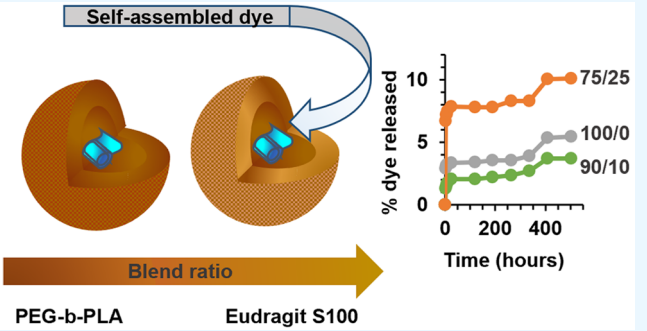

1. INTRODUCTION

Organic dyes are increasingly being explored as valuable components for bioimaging, disease diagnosis, photodynamic therapy, and photothermal therapy.[1,2] A large collection of organic dyes are also known for their pharmacological properties in the treatment of diseases including cancer, brain disorders, and different types of infections.[3,4] Hence, combining organic dye-based materials with a nanotechnology approach has been considered an emerging tool in nanomedicine.[5] In this regard, different strategies have been studied for the encapsulation of dye molecules with polymers and other encapsulating agents to increase diagnosis efficiency and treatment modalities.[6,7] These encapsulated dye nanostructures showed the ability to carry dye substances, separating them from the outer environment followed by controlled release.

Among a variety of encapsulated dye nanostructures, polymeric nanocapsules have been widely applied due to their core−shell structure that offers material architecture-based diverse structures in delivering organic dyes.[8−10] Commonly, the nanocapsule shell acts as a diffusion barrier, while the capsule cavity core, defining the interior nanospace, has been applied to encapsulate dye molecules. For example, cyanine dye was loaded in poly(D,L-lactide) and polycaprolactone nanocapsules by the nanoprecipitation method[11] and dispersed red 1 dye was encapsulated in poly(methyl methacrylate) nanocapsules using the phase separation method.[12] Other structures of polymeric nanocapsules loaded by dye molecules can be obtained by electrostatic attractions between the polymeric material and the dye molecules by utilizing a layer-by-layer deposition method. In these nanocapsule structures, either exterior or interior surfaces of the shell are used as the template and scaffold for the adsorbed dyes.[13] In another variation, the dye can be embedded into the shell matrix by mixing with a polymer during the nanocapsule formation[14] or through its conjugation to end functional groups of the polymer prior to the preparation.[15,16] The interplay between dye molecules and the polymeric material as well as the fabrication method influences the resulting dye−polymeric nanocapsule configuration.[17,18]

Received: December 28, 2023
Revised: February 5, 2024
Accepted: February 19, 2024
Published: March 5, 2024

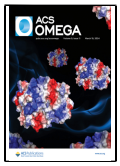

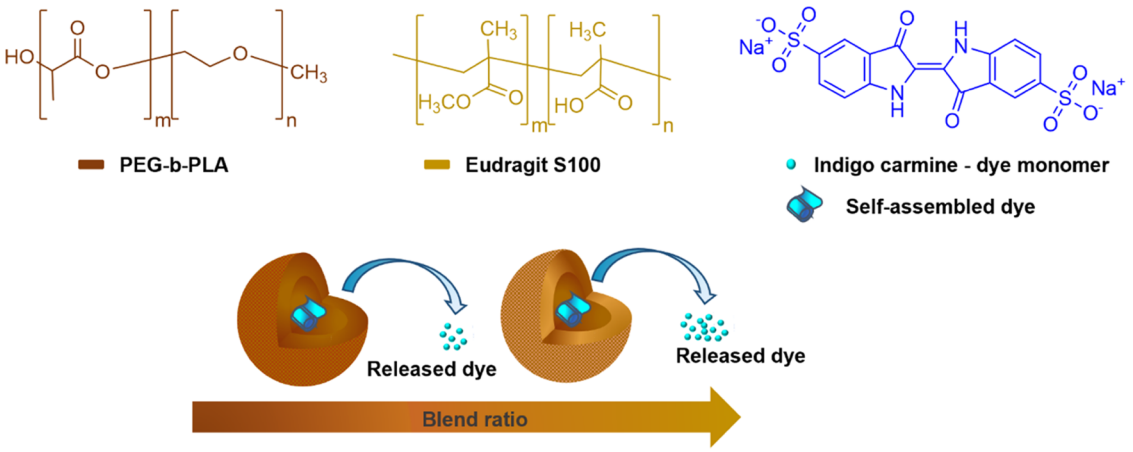

Figure 1. Structural representations of the encapsulating agents and the encapsulated dye used in this study and a schematic illustration of polymer blend composition effects. Inside the capsule is shown a graphical representation of a self-assembled nanoscroll of indigo carmine obtained by encapsulating the dye monomers.

Recently, we showed that the polymeric nanoshell has another critical role in providing a confining environment with highly ordered spherical geometry.[19] As demonstrated, the ability of an organic dye such as indigo carmine (IC) to self-assemble into organized structures was strongly related to the confining space defined by the capsule shell. Apparently, a local high concentration of IC molecules was yielded in the cavity capsules, enhancing their tendency to assemble and form a stable lamellar sheet. Finally, the sheet rolled to a scroll-like structure dictated by the polymeric shell restriction. This process was obtained by taking an encapsulation approach to entrap water-soluble substances within the aqueous core of hydrophobic nanocapsules, namely, the water-in-oil-in-water ($W_1/O/W_2$) double emulsion method.[20] The model dye IC has already been established as a suitable agent in a wide variety of applications[21] including as a diagnostic tool in clinical medicine.[22−24] The encapsulating material was based on a solution blend of two biocompatible polymers that could form a negatively charged interior wall. Specifically, the binary blend was composed of poly(ethylene glycol)-*block*-poly(D,L-lactic acid) (PEG-*b*-PLA with PEG and PDLLA molecular weights of 5 and 100 kDa, respectively) with 10% w/w Eudragit S100 (1:2 copolymer of methacrylic acid and methyl methacrylate).

Polylactic acid and its blends with other polymers have attracted massive attention in the quest for better materials needed in food packing, pharmaceutical, and biomedical applications.[25−28] Poly(ethylene glycol) (PEG) is commonly used as a hydrophilic block to create a hydrated steric barrier, which helps to enhance blood circulation time.[29,30] Hence, block copolymers based on PEG-*b*-PLA are being studied for drug delivery systems such as nanocapsules,[31] nanospheres,[32] polymersomes,[33] and micelles.[34] The polyanionic copolymer Eudragit S100 is also widely used as a functional component for controlled-release systems,[35] associated with a higher relative content of anionic residues across the polymer backbone.[36,37] Generally, polymeric blends exhibit technological advantages, which make them suitable materials for various biomedical applications.[38,39]

Nevertheless, the intermolecular interactions in the mixture of PEG-*b*-PLA (PEG block MW: 5 kDa, PDLLA block MW: 100 kDa) and Eudragit S100 have not been studied previously to the best of our knowledge. In this context, the encapsulation of anionic dye molecules (i.e., IC) may be tuned by the interplay between the anionic character of the interior polymeric wall and the miscibility of the polymers with one another. Hence, an increase of Eudragit S100, which has a higher anionic character, should result in higher repulsion of the entrapped IC molecules, thus leading to a self-assembly at a lower critical concentration inside the capsule core. However, due to the possibility of limited miscibility of Eudragit S100 in the studied PEG-*b*-PLA, we also anticipate an influence on the nanoparticle morphology, the formation of a self-assembled structure, and the dye release behavior (Figure 1).

In the present work, binary blends were prepared by solution mixing at different PEG-*b*-PLA/Eudragit S100 ratios (namely, 100/0, 90/10, 75/25, and 50/50% w/w). The solution blends served as encapsulating agents for the IC organic dye nanoencapsulation. The obtained formulations were characterized in terms of particle size, surface charge, and dye entrapment. The effect of the Eudragit S100 amount in the dye formulations was examined by Fourier transform infrared spectroscopy (FTIR), thermogravimetric analysis (TGA), and differential scanning calorimetry (DSC), allowing the evaluation of intermolecular interactions and thermal properties. Finally, pH-dependent in vitro dye release profiles were considered.

2. EXPERIMENTAL SECTION

2.1. Materials. Indigo carmine, poly(vinyl alcohol) (PVA, MW 30−70 kDa), HPLC-grade dichloromethane (DCM), HPLC-grade water, and phosphate-buffered saline (PBS) were all purchased from Sigma-Aldrich Chemicals (Israel). Methoxy-poly(ethylene glycol)-*block*-poly(D,L-lactic acid) (PEG-*b*-PLA with 5 kDa PEG and 100 kDa PDLLA) was purchased from Jinan Daigang Biomaterial Co., Ltd. (China). The Eudragit S100 copolymer was obtained from Evonik Röhm GmbH (Germany).

2.2. Encapsulation Procedure. Encapsulated IC formulations at different PEG-*b*-PLA/Eudragit S100 ratios (100/0, 90/10, 75/25, and 50/50% w/w) were synthesized using the following encapsulation procedure, which is described in detail in Maor et al.[19] Binary blends were prepared from a solution of PEG-*b*-PLA in DCM (1% w/v) with Eudragit S100 in DCM (1% w/v) added dropwise under stirring. Briefly, an aqueous solution of IC (1 mL, 2.5% w/v) was emulsified in DCM

https://doi.org/10.1021/acsomega.3c10447
ACS Omega 2024, 9, 13382−13390

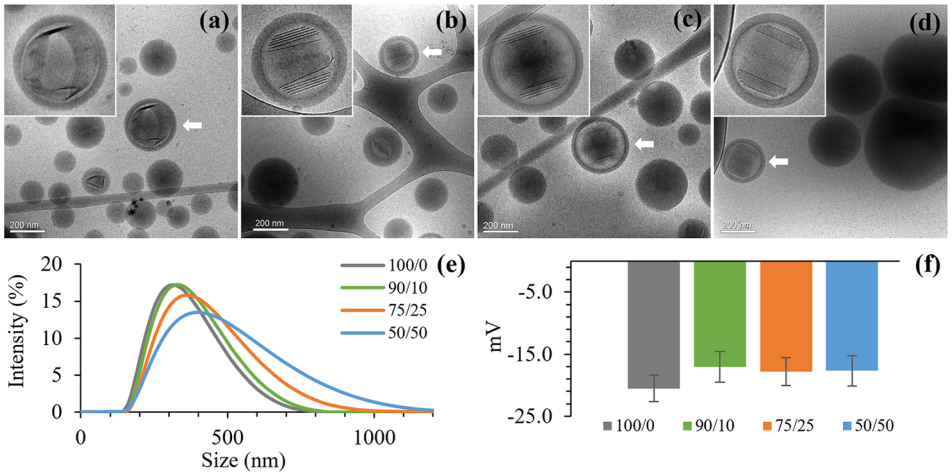

Figure 2. Characterization of dye-encapsulated PEG-*b*-PLA/Eudragit S100 blend particles: cryogenic-TEM images (a) 100/0, (b) 90/10, (c) 75/25, and (d) 50/50; the arrow points to a single nanocapsule within a self-assembled IC structure. The inset shows a close-up image of the same nanocapsules. The scale bar corresponds to 200 nm. (e) Size distribution histograms by DLS, and (f) ζ-potential measurement.

containing the PEG-*b*-PLA or PEG-*b*-PLA/Eudragit S100 mixture (10 mL, 1% w/v) using a probe-type sonication (1 min, 10 s on/off mode) in an ice-water bath. The formed W_1/O emulsion was immediately dispersed with a high concentration of PVA aqueous solution (10 mL, 1% w/w) and this was emulsified under the same conditions to form the double emulsion ($W_1/O/W_2$). Then, the emulsion was poured into a low concentration of PVA aqueous solution (180 mL, 0.1% w/w), and the organic solvent was allowed to evaporate, yielding solidification of the nanoparticles. The nanoparticle formulation was collected by centrifugation (8000 rpm, 20 min) and washed with water to remove the nonencapsulated dye and surfactant. Finally, the pellet was redispersed in water and kept at 4 °C until further use.

2.3. Characterization Techniques. Particle size distribution (hydrodynamic diameter and polydispersity index) and surface charge (ζ-potential) were determined by using a dynamic light scattering (DLS) Zetasizer Nano ZS (Malvern Panalytical, U.K.). The results represent the mean and standard deviation of representative batches ($n = 3$). Cryogenic transmission electron microscopy (cryo-TEM) was carried out using a Tecnai T12 G2 TEM (FEI Technologies Inc., Oregon) equipped with a LaB_6 electron gun operated at 120 kV. Images were taken digitally by a Gatan US 1000 high-resolution CCD camera using DigitalMicrograph software (Tecnai T-12). Attenuated total reflectance Fourier transform infrared (ATR-FTIR) spectroscopy analysis was conducted using a Nicolete-iS50 (Thermo Scientific). The spectra were scanned between 400 and 4000 cm^{-1} with a resolution of 4 cm^{-1}. Ultraviolet−visible (UV−vis) absorbance spectra were measured using an Ultrospec 2100 pro UV/vis spectrophotometer (Biochrom Ltd., U.K.). The thermal stability of samples was obtained using a Q500 thermogravimetric analyzer (TA Instruments). Thermogravimetric analysis (TGA) was carried out between 35 and 600 °C at a heating rate of 10 °C/min under a nitrogen atmosphere. Differential scanning calorimetry (DSC) measurements were performed using the DSC 3+ modulus (Mettler-Toledo GmbH, Analytical), in the range between 0 and 180 °C, at the rate of 10 °C/min under a nitrogen atmosphere.

2.4. Analysis of the Dye Content. The IC loading was determined by stirring 0.5 mL of the aqueous suspension of the dye formulation sample mixed in 3 mL of DCM overnight. After the dissolution of polymers, the concentration of the nonentrapped IC in the aqueous phase was measured spectrophotometrically at 610 nm using a standard calibration curve.[40]

2.5. In Vitro Dye Release Study. The profiles of dye release from nanoparticle formulations of three blends (100/0, 90/10, and 75/25% w/w) were studied in phosphate-buffered saline (PBS, pH 7.4) or acidic PBS with HCl (pH 1.8 and 4.3). Specifically, nanoparticle samples containing IC (1.5 mL of release medium, 0.2 mg of IC/mL) were placed in an orbital shaker rotating at 140 rpm and kept at 37 °C. Samples taken at time intervals were centrifuged at 8000 rpm for 5 min. Then, 1 mL of supernatant was removed, and fresh replacement medium (1 mL) was added to resuspend the particles to maintain the sink condition. The concentration of IC in the collected media was analyzed spectrophotometrically at 610 nm. The cumulative dye release at each time interval was calculated. All studies were performed in triplicate, and data were expressed as the mean value ± standard deviation. Different mathematical models were applied to describe the release kinetics of IC from the polymeric formulations by fitting the release data to four kinetic equations: zero-order, first-order, Higuchi, and Korsmeyer−Peppas models.[41]

3. RESULTS AND DISCUSSION

3.1. Encapsulation of Indigo Carmine in PEG-*b*-PLA/Eudragit S100 Blends. By variation of the amount of Eudragit S100 in the PEG-*b*-PLA-based blends serving as encapsulating agents, its effects on the success of the IC encapsulation were initially explored. Four encapsulated dye formulations were obtained at different PEG-*b*-PLA to Eudragit S100 weight ratios (100/0, 90/10, 75/25, and 50/50% w/w). The cryogenic TEM imaging, regardless of the Eudragit S100 amount in the blends, revealed nanocapsules loaded with prominent structural self-assembled elements of IC, such as rolled-up sheets forming tubular scrolls (Figure 2a−d). We recently described in detail the self-assembling process of IC molecules in the confined cavities of nanocapsules.[19] One important observation is that if entrapped in nanocapsule cores above a certain critical concentration, IC molecules form self-organized structures. In this work, it was

https://doi.org/10.1021/acsomega.3c10447
ACS Omega 2024, 9, 13382−13390

noticed that the addition of a small amount of anionic Eudragit S100 to PEG-*b*-PLA improved the encapsulation efficiency and loading capacity. For example, an encapsulated dye formulation composed of 10% Eudragit S100 exhibited 5.3 ± 1.3% encapsulation efficiency (EE) and 2.1 ± 0.9% loading capacity (LC) of IC. However, increasing the amount of Eudragit S100 in the blend (i.e., 25%) reduced these values. Moreover, due to the very low amount of encapsulated IC, as reflected by the significantly low encapsulation efficiency and loading capacity values (Table 1), only a few self-assembled structures appeared in the 50/50 blend (by TEM). The obtained results imply that the anionic copolymer Eudragit S100 in the blend has an influence on the IC entrapment process in a composition-dependent manner.

Table 1. Nanoparticle Formulations of the Encapsulated Dye with Different Ratios of PEG-b-PLA/Eudragit S100 (% w/w)

formulation	particle size[a] (nm)	PDI[a]	EE[b] (%)	LC[c] (%)
100/0	318 ± 26	0.152 ± 0.010	2.4 ± 0.5	1.2 ± 0.5
90/10	333 ± 24	0.138 ± 0.049	5.3 ± 1.3	2.1 ± 0.9
75/25	349 ± 11	0.140 ± 0.016	2.1 ± 1.0	1.0 ± 0.6
50/50	366 ± 29	0.198 ± 0.051	0.5 ± 0.3	0.3 ± 0.2

[a]Data were determined by DLS as the *z*-average hydrodynamic diameter. [b]EE (%) = (weight of encapsulated IC)/(weight of total IC loaded) × 100. [c]LC (%) = (weight of encapsulated IC)/(weight of the IC formulation) × 100.

The *z*-average hydrodynamic diameter of each dye formulation was evaluated by dynamic light scattering (DLS). The particle size ranged from 318 to 366 nm as a function of the amount of Eudragit S100 in the blend (Table 1). The smallest particles were obtained without the addition of Eudragit S100. With a decrease in the PEG-*b*-PLA-to-Eudragit S100 ratio, both the average diameter and polydispersity index (PDI) of the particles increased (Figure 2e). This trend was previously described in the series of nanoparticles made by low-molecular weight PLLA, Eudragit S100, and their blend.[42] In addition to particle size, changes in ζ-potential were observed when compared with the Eudragit S100 free formulation (Figure 2f). Due to the encapsulating polymers' structure, all formulations showed negative ζ-potential values, as expected.[43−45] The PEG-*b*-PLA nanoparticle formulation (100/0) showed a slightly higher negative charge (−20.5 ± 2.1 mV) than that of the PEG-*b*-PLA/Eudragit S100 formulations (−17.1 ± 2.5, −17.8 ± 2.3, and −17.7 ± 2.4 mV for 90/10, 75/25, and 50/50 of PEG-*b*-PLA to Eudragit S100, respectively). The slight changes suggest that the PEG-*b*-PLA chains are partially surrounded by acidic functional groups of Eudragit S100, which lead to a less negative surface charge.

3.2. Fourier Transform Infrared Spectroscopy Analysis. To evaluate intermolecular interactions between PEG-b-PLA and Eudragit S100 in the nanoparticle formulations obtained from dye encapsulation, FTIR spectroscopy was used to detect changes in the vibrational frequencies of specific functional groups. The absorbance spectra of encapsulated IC formulations were compared to those of neat polymers and IC. The results are shown in Figures 3 and Supporting Information Figure S1, and the major bands are summarized in Table 2. The analysis showed distinct features of PEG-b-PLA in all formulation spectra, and peak locations were consistent with previous studies.[46] The characteristic bands of Eudragit S100 were clearly observed in the spectrum of the 50/50 formulation (Figure 3a) and appeared as a shoulder peak with a decrease in the Eudragit S100 fraction (Figure 3c,d). The IC bands were not observed in the dye formulation spectra, and this may be associated with the low loading capacity (Table 1). The effect of Eudragit S100 addition was

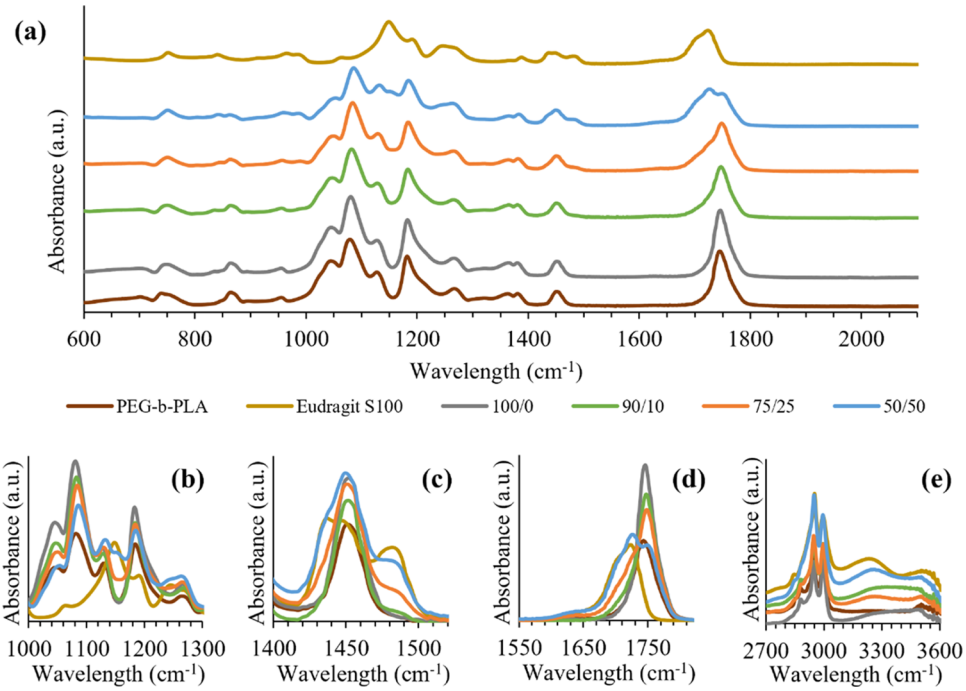

Figure 3. (a) ATR-FTIR spectra of nanoparticle formulations of the encapsulated dye with different ratios of PEG-*b*-PLA/Eudragit S100 (% w/w). The inset shows selected regions: (b) 1000−1300 cm^{-1}, (c) 1400−1520 cm^{-1}, (d) 1550−1820 cm^{-1}, and (e) 2700−3600 cm^{-1}.

https://doi.org/10.1021/acsomega.3c10447
ACS Omega 2024, 9, 13382−13390

Table 2. Comparison of the Major Bands in the ATR-FTIR Spectra[a]

assignment	wavenumber (cm^{-1})					
	PEG-*b*-PLA	100/0	90/10	75/25	50/50	Eudragit S100
ν_sC−O−C	1081	1081	1082	1084	1086	
ν_{as}C−O−C	1182	1182	1183	1184	1184	1190
$\delta_{as}CH_3$	1451	1451	1451	1451	1451 sh	1482
νC═O methyl methacrylate					1726	1723 br
νC═O lactide ester	1745	1746	1747	1748	1748	
ν_sCH_3, $\nu_{as}CH_3$	2945, 2995	2945, 2995	2946, 2995	2947, 2995	2949, 2995	2951, 2995
νO−H free hydroxyl hydrogen-bonded			3269−3547 br	3267−3547 br	3260, 3547	3233, 3547

[a]sh = shoulder; br = broad; s = symmetric; and as = asymmetric.

indirectly analyzed on the prominent bands of PEG-b-PLA. The ester groups of the polylactide backbone show three strong stretching vibrations related to C═O and C−O−C assigned to 1745, 1182, and 1081 cm^{-1} (Table 2). The isolated carbonyl regions (Figure 3b,3d) show a slight shift of these bands toward higher wavenumbers as a function of the PEG-b-PLA to Eudragit S100 ratio in the polymer composition. The predominant change was observed for the stretching vibration of the ether−ester oxygen bond at 1081 cm^{-1}, which shifted to 1086 cm^{-1} with the increase of Eudragit S100 (Table 2). In addition, the spectrum of the 50/50 formulation exhibited two maxima at 1748 and 1726 cm^{-1} attributed to the C═O stretching vibration of PEG-b-PLA and Eudragit S100, respectively, both blue-shifted ($\Delta\nu$ = 3 cm^{-1}) with respect to the neat polymers. Clearly, the blending of Eudragit S100 and PEG-*b*-PLA caused a blue shift of the ester bands. Moreover, the spectrum of Eudragit S100 showed maxima attributed to the intermolecular hydrogen-bonded hydroxyl stretching mode (self-associated carboxylic groups) and intramolecular hydrogen-bonded hydroxyl stretching mode ("free" hydroxyl) at 3233 and 3547 cm^{-1} ($\Delta\nu$O−H = 314 cm^{-1}), respectively (Figure 3e). It can be observed that the free hydroxyl peaks in the blends occurred in the same position as in the neat polymer, whereas the self-association peaks were blue-shifted (e.g., $\Delta\nu$O−H = 287 cm^{-1} for the 50/50 formulation). These results suggest weak intermolecular interactions between the two polymers in the context of hydrogen bonding between the proton donor groups of carboxylic acid moieties in Eudragit S100 and the proton acceptor groups such as lactide ester groups. The intermolecular hydrogen bonding formation is considered a good predictor for miscibility of blends.[47] Therefore, it can be expected that with such a weak hydrogen bonding network, PEG-b-PLA and Eudragit S100 are less likely to form a miscible blend with each other in all weight ratios.

3.3. Thermal Analysis. To examine the compositional effect of PEG-*b*-PLA/Eudragit S100 blends on their miscibility, the glass transition temperatures (T_g) of the samples were measured using differential scanning calorimetry (DSC). Figure 4 shows the glass transition region of PEG-*b*-PLA and Eudragit S100 as a function of their composition in the encapsulated IC formulation. The T_g value of the PEG-*b*-PLA phase in the nanoparticle formulation (i.e., 100/0) was shifted slightly to higher temperatures compared to amorphous neat PEG-*b*-PLA. A similar DSC result was observed for drug (paclitaxel)-loaded PLDLA microspheres.[48] Upon blending with Eudragit S100, the T_g values of the PEG-*b*-PLA phase became higher. A single T_g was found in the formulation containing 10% Eudragit S100, indicating that the polymers in the blend are miscible. Formulations containing 25 and 50% Eudragit S100 showed two T_g values that were located between

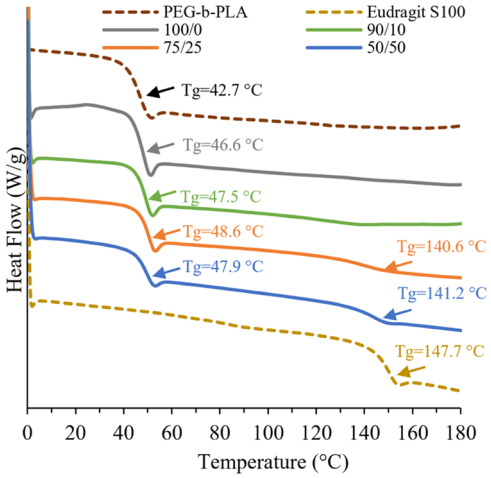

Figure 4. Plot of heat flow against temperature in the glass transition temperature range for nanoparticle formulations of the encapsulated dye with different ratios of PEG-*b*-PLA/Eudragit S100 (% w/w).

the values assigned to the neat polymers. Hence, a higher content of Eudragit S100 in the blend decreases the miscibility of the two polymers, forming a more heterogeneous spatial arrangement of the phases.

Furthermore, a thermal study of IC encapsulated in the nanoparticle formulation was carried out by thermogravimetric (TG) and differential thermal analysis (DTA) measurements, and the results are presented in Figure 5 and Table 3. The encapsulated IC formulations comprising polymeric mixtures exhibited two successive decomposition stages with the rise of the temperature. The mass loss (Δw) values changed in accordance with the polymer ratio in the encapsulating matrix, indicating that the decomposition of PEG-*b*-PLA occurs initially and is followed by that of Eudragit S100. Neat PEG-*b*-PLA was thermally degraded from 258 to 411 °C with the maximum degradation temperature (T_{max}) observed at 358 °C. The entrapment of the IC dye using the encapsulation process induced a significant difference in PEG-*b*-PLA thermal stability since the initial decomposition temperature (T_i) was shifted to a lower temperature (189 °C). A similar reduction of PLA thermal stability has been described in the presence of lignin, which was attributed to the action of its phenolic hydroxyl and carboxylic groups.[49] Regardless of encapsulating materials used, the TGA of all encapsulated IC formulations exhibited a similar amount of residue (~5.0%), which could be partially related to the total IC content in the sample as the T_i value of IC is at 427 °C[50,51] (Supporting Information Figure S1). T_i values were increased (239−232 °C) with the addition of Eudragit S100 as a component in the encapsulating agent, as

https://doi.org/10.1021/acsomega.3c10447
ACS Omega 2024, 9, 13382−13390

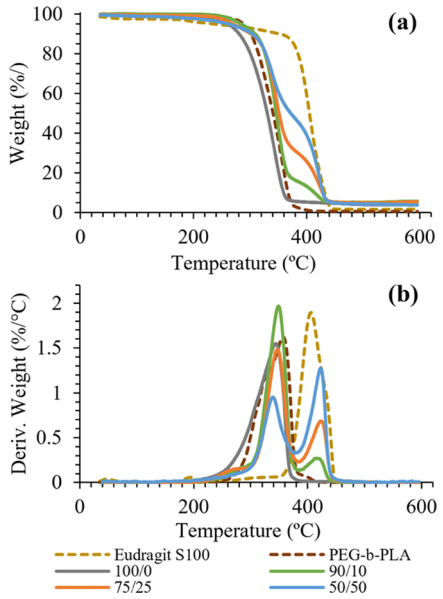

Figure 5. (a) TG and (b) DTG curves of nanoparticle formulations of the encapsulated dye with different ratios of PEG-*b*-PLA/Eudragit S100 (% w/w).

seen in Table 3. Furthermore, T_{50} increased from 330 °C for the IC formulation made by PEG-*b*-PLA (100/0) to 347, 351, and 371 °C for formulations containing 10, 25, and 50% Eudragit S100, respectively. The increase of thermal stability with the increase of the Eudragit S100 amount could be associated with the mobility restriction of PEG-*b*-PLA chains imposed by Eudragit S100, eventually hindering the degradation of nanoparticle formulations containing Eudragit S100.

3.4. Dye Release Profiles. The release properties of PEG-*b*-PLA/Eudragit S100 blends were studied under different pH conditions for 3 weeks. Figure 6 shows the time dependence of cumulative IC release from the 100/0, 90/10, and 75/10 formulations, which revealed similar release patterns. The release of IC from the nanoparticles involved an initial rapid-release phase, followed by a relatively slow-release phase (Figure 6a–c). However, the amount of dye released in the initial burst stage was strongly affected by the amount of Eudragit S100 in the blend (Figure 6d). As shown, IC release was the slowest from the 90/10 formulation and the fastest from the 75/25 formulation compared to the PEG-*b*-PLA formulation (100/0). For example, at the initial stage (pH 7.4), the fractions of dye released from 100/0, 90/10, and 75/25 formulations were 3.2, 1.8, and 7.5%, respectively. These release profiles can be correlated with the T_g values gained from DSC analysis.[52] The two polymers, PEG-*b*-PLA and Eudragit S100, are miscible at a 90/10 ratio, characterized as a homogeneous blend with a single higher T_g value, indicating a reduction in chain mobility. Hence, the shell matrix of nanocapsules composed at this polymer blend ratio helps in the prevention of IC leakage. The 75/25 blend ratio was found to be partially miscible, which is corroborated by the FTIR and TGA results, indicating that weak intermolecular interactions between Eudragit S100 and PEG-*b*-PLA are predominating. Consequently, a loose interface may form between the two polymers, leading to a less compact structure of the encapsulating polymer matrix that could induce a higher burst release of the IC.

Eudragit S100 is a pH-dependent polymer and insoluble in dissolution medium with a pH less than 7. While PLA is a polyester that can be degraded through hydrolysis under acidic and basic conditions, it demonstrates relatively slow hydrolysis at a pH of about 4 as the pK_a of lactic acid is 3.84.[53] Hence, all dye formulations exhibited only a slight burst of IC release followed by a very slow release rate at pH 4.3 (Figure 6b). The dye release mechanisms for dye formulations under high- and low-pH conditions were evaluated by applying various release kinetic models (Table 4). At pH 7.4, the correlation coefficient values for fitting the release profiles to the mathematical model for the encapsulated IC formulation made by PEG-*b*-PLA (100/0) are in good agreement with first-order kinetics (R^2 = 0.8642). This suggests that the release mechanism is mainly controlled by surface erosion, as previously reported for the poly(D,L-lactide) microsphere drug release mechanism.[54] With the addition of Eudragit S100, the erosion-controlled mechanism was retained at pH 7.4, showing a good correlation with first-order kinetics as well, i.e., R^2 = 0.8858 and R^2 = 0.8467 for formulations containing 10 and 25% Eudragit S100, respectively. These results can be associated with the increased swelling and erosion of PLA due to Eudragit S100 becoming more permeable, along with the dissociation of methacrylic groups at pH 7.4.[55] A similar observation is reported in the literature for nanoparticle formulations with a different ratio of PLGA(RG756)/Eudragit S100 nanoparticles.[56] However, under acidic conditions (pH 1.8), the formulation containing 10% Eudragit S100 exhibited IC release best fitted to the Higuchi order (R^2 = 0.9423), suggesting a diffusion-controlled mechanism of IC release. Fitting the release pattern to the Korsmeyer–Peppas model showed R^2 = 0.9676 and R^2 = 0.8185 for formulations containing 10 and 25% Eudragit S100, respectively (Table 4). The n values (the diffusional exponent) were smaller than 0.5, indicating a Fickian diffusion pattern. Hence, the mechanism may be governed by diffusion more than relaxation. These results can be rationalized under acidic

Table 3. Thermal Analysis Parameters[a]

	stage 1				stage 2					
sample	T_i (°C)	T_{max} (°C)	T_f (°C)	Δw (%)	T_i (°C)	T_{max} (°C)	T_f (°C)	Δw (%)	Δw_{res} (%)	T_{50} (°C)
PEG-*b*-PLA	258	358	411	98					0.9	340
100/0	189	346	384	94					5.6	330
90/10	239	351	383	84	384	413	443	11	5.5	347
75/25	232	349	382	68	383	428	445	25	5.5	351
50/50	232	344	380	50	381	425	449	42	5.0	371
Eudragit S100	345	407	449	95					1.8	405

[a] T_i: onset temperature, T_{max}: temperature corresponding to the maximum rate of mass loss, T_f: final temperature, Δw: mass loss in the range of T_i–T_f, Δw_{res}: weight residues, and T_{50}: temperature corresponding to the 50% of sample mass loss.

https://doi.org/10.1021/acsomega.3c10447
ACS Omega 2024, 9, 13382–13390

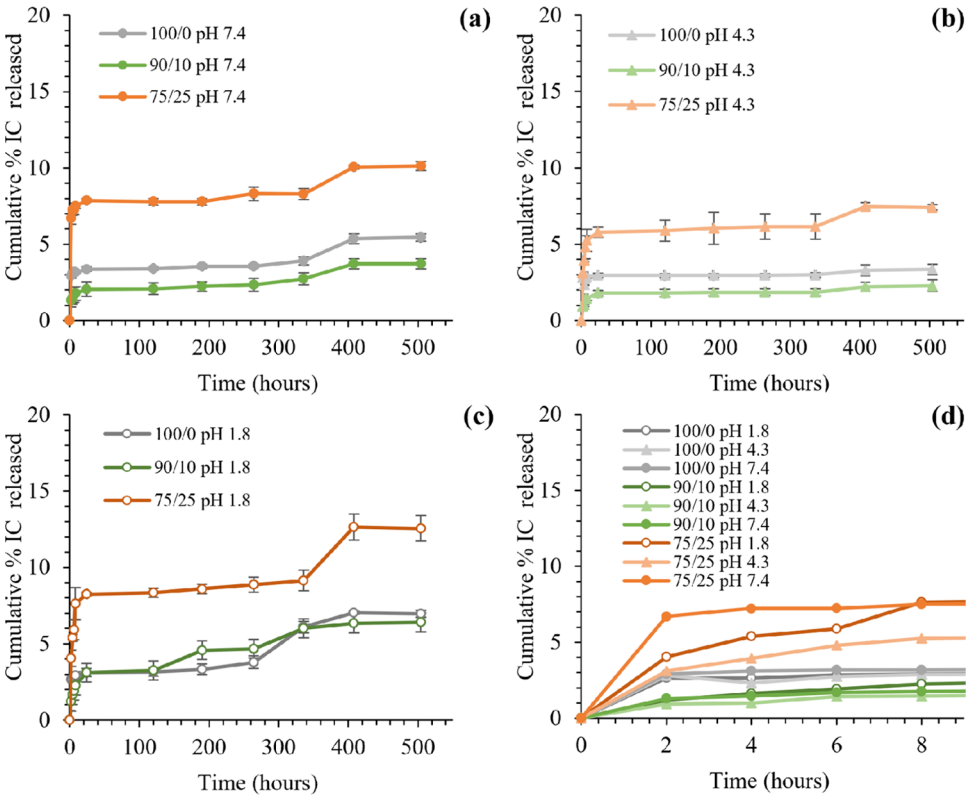

Figure 6. IC release profiles of the nanoparticle formulations in PBS at 37 °C with different pH values: (a) pH 7.4, (b) pH 4.3, (c) pH 1.8, and (d) the initial 8 h (the error bars are omitted for clarity).

Table 4. Fitting Release Kinetic Models to IC Release Data

	model (R^2)			
formulation	zero-order	first-order	Higuchi	Korsmeyer–Peppas (n)[a]
100/0, pH 7.4	0.5614	0.8642	0.5915	0.6159 (0.0784)
90/10, pH 7.4	0.7604	0.8858	0.7905	0.8356 (0.1487)
75/25, pH 7.4	0.3697	0.8467	0.4463	0.6969 (0.0517)
100/0, pH 1.8	0.8006	0.9111	0.7717	0.6639 (0.1493)
90/10, pH 1.8	0.8716	0.8039	0.9423	0.9676 (0.2722)
75/25, pH 1.8	0.6524	0.6959	0.7315	0.8185 (0.1475)

[a]Release exponent evaluated for n < 15% released.

conditions in which Eudragit S100 is insoluble and characterized by low permeability because of strong hydrogen bonding,[56] while PLA exhibits accelerated hydrolytic degradation.[57] This may be followed by the appearance of channels and pores within the polymer shell matrix, facilitating diffusion of the IC to the medium and inevitably enhancing dye release. In summary, differences in release behavior observed in the above media underline the importance of testing the *in vitro* release, revealing the impact of a tunable amount of Eudragit S100 on preventing premature leakage and controlled release of IC dye.

4. CONCLUSIONS

The nanocapsule shell plays a critical role in providing constraints that limit, direct, and control the self-assembly growth of the encapsulated IC organic dye. The blending of encapsulating agents such as PEG-*b*-PLA and Eudragit S100, at certain ratio limits, provides sufficient accumulation of IC molecules in the nanocapsule core to form the scrolled structures. Furthermore, under the conditions of the entrapment process by the $W_1/O/W_2$ double emulsion, the Eudragit S100 is in a mostly dissociated form, meaning that it possesses negative charges that favorably direct the anionic dye IC molecules by electrostatic repulsion. At the same time, increasing the Eudragit S100 fraction disrupted the chain packing of the shell matrix due to weak intermolecular interactions between the two polymers, as indicated by observable changes in the FTIR spectra. The results of TGA and DSC corroborated these observations and showed changes in intermolecular packing and the miscibility of the polymer blends. The optimal interplay of properties was found in the formulations containing 10 and 25% Eudragit S100. However, the 90/10 formulation had a single phase (single T_g at 47.5 °C); therefore, it is considered a miscible blend, while the 75/25 formulation, forming two distinct phases (two T_g values at 48.6 and 140.6 °C), is a partially miscible blend. A miscible blend like the 90/10 blend ratio is preferable, as it forms a more packed shell matrix with low chain mobility, resulting in less IC leakage and a slower release rate (about 3.7% at pH 7.4 within 21 days). The results offer insights into the properties of these polymer blends, which are important for accelerating the rational design of polymeric core–shell structures delivering organic dyes for therapeutic and diagnostic purposes.

■ ASSOCIATED CONTENT

Supporting Information

The Supporting Information is available free of charge at https://pubs.acs.org/doi/10.1021/acsomega.3c10447.

Characterization of indigo carmine: FTIR and TGA (PDF)

https://doi.org/10.1021/acsomega.3c10447
ACS Omega 2024, 9, 13382−13390

AUTHOR INFORMATION

Corresponding Author

Iris S. Weitz − *Department of Biotechnology Engineering, Braude College of Engineering Karmiel, Karmiel 2161002, Israel;* orcid.org/0000-0002-5445-6607; Email: irisweitz@braude.ac.il

Authors

Shaked Ashkenazi − *Department of Biotechnology Engineering, Braude College of Engineering Karmiel, Karmiel 2161002, Israel*

Pnina Matsanov − *Department of Biotechnology Engineering, Braude College of Engineering Karmiel, Karmiel 2161002, Israel*

Eid Nassar-Marjiya − *The Laboratory for Advanced Functional/Medicinal Polymers & Smart Drug Delivery Technologies, The Wolfson Faculty of Chemical Engineering, Technion − Israel Institute of Technology, Haifa 3200003, Israel*

Shady Farah − *The Laboratory for Advanced Functional/Medicinal Polymers & Smart Drug Delivery Technologies, The Wolfson Faculty of Chemical Engineering, Technion − Israel Institute of Technology, Haifa 3200003, Israel; The Russell Berrie Nanotechnology Institute, Technion − Israel Institute of Technology, Haifa 3200003, Israel*

Complete contact information is available at: https://pubs.acs.org/10.1021/acsomega.3c10447

Author Contributions

‖S.A. and P.M. contributed equally. The article was written through contributions of all authors. All authors have given approval to the final version of the article.

Notes

The authors declare no competing financial interest.

ACKNOWLEDGMENTS

The authors are grateful for financial support from the Braude College Research Committee. S.F. was supported by an MAOF Fellowship from the Council for Higher Education, Israel. The authors would like to thank Dr. Ellina Kesselman for assistance with cryogenic-TEM imaging (Center for Electron Microscopy of Soft Matter, Technion—Israel Institute of Technology Israel). The authors thank Dr. Krishanu Ghosal for assistance with the DSC analysis (The Wolfson Faculty of Chemical Engineering, Technion—Israel Institute of Technology, Israel). The authors also want to thank Inbal Maor, who helped with the analyses as a part of her research project (Department of Biotechnology Engineering, Braude College of Engineering Karmiel, Israel).

ABBREVIATIONS

PEG-*b*-PLA, methoxy-poly(ethylene glycol)-*block*-poly(D,L-lactic acid); IC, indigo carmine

REFERENCES

(1) Ji, C.; Lai, L.; Li, P.; Wu, Z.; Cheng, W.; Yin, M. Organic dye assemblies with aggregation-induced photophysical changes and their bio-applications. *Aggregate* **2021**, *2* (4), No. e39.

(2) Cheng, W.; Chen, H.; Liu, C.; Ji, C.; Ma, G.; Yin, M. Functional organic dyes for health-related applications. *VIEW* **2020**, *1* (4), No. 20200055.

(3) Yaneva, Z.; Ivanova, D.; Nikolova, N.; Toneva, M. Organic dyes in contemporary medicinal chemistry and biomedicine. I. From the chromophore to the bioimaging/bioassay agent. *Biotechnol. Biotechnol. Equip.* **2022**, *36* (1), 1−14.

(4) Yadav, S.; Tiwari, K. S.; Gupta, C.; Tiwari, M. K.; Khan, A.; Sonkar, S. P. A brief review on natural dyes, pigments: Recent advances and future perspectives. *Results Chem.* **2023**, *5*, No. 100733.

(5) Cai, Y.; Si, W.; Huang, W.; Chen, P.; Shao, J.; Dong, X. Organic dye based nanoparticles for cancer phototheranostics. *Small* **2018**, *14* (25), No. 1704247.

(6) Yin, X.; Cheng, Y.; Feng, Y.; Stiles, W. R.; Park, S. H.; Kang, H.; Choi, H. S. Phototheranostics for multifunctional treatment of cancer with fluorescence imaging. *Adv. Drug Delivery Rev.* **2022**, *189*, No. 114483.

(7) Mamidi, N.; Velasco Delgadillo, R. M.; Barrera, E. V.; Ramakrishna, S.; Annabi, N. Carbonaceous nanomaterials incorporated biomaterials: The present and future of the flourishing field. *Composites, Part B* **2022**, *243*, No. 110150.

(8) Frank, L. A.; Contri, R. V.; Beck, R. C. R.; Pohlmann, A. R.; Guterres, S. S. Improving drug biological effects by encapsulation into polymeric nanocapsules. *WIREs Nanomed. Nanobiotechnol.* **2015**, *7* (5), 623−639.

(9) Kothamasu, P.; Kanumur, H.; Ravur, N.; Maddu, C.; Parasuramrajam, R.; Thangavel, S. Nanocapsules: the weapons for novel drug delivery systems. *Bioimpacts* **2012**, *2* (2), 71−81.

(10) Dergunov, S. A.; Kim, M. D.; Shmakov, S. N.; Pinkhassik, E. Building functional nanodevices with vesicle-templated porous polymer nanocapsules. *Acc. Chem. Res.* **2019**, *52* (1), 189−198.

(11) Bazylińska, U.; Lewińska, A.; Lamch, Ł.; Wilk, K. A. Polymeric nanocapsules and nanospheres for encapsulation and long sustained release of hydrophobic cyanine-type photosensitizer. *Colloids Surf., A* **2014**, *442*, 42−49.

(12) Sharifimehr, M. R.; Ghanbari, K.; Ayoubi, K.; Mohajerani, E. Preparation and spectral characterization of polymeric nanocapsules containing DR1 organic dye. *Opt. Mater.* **2015**, *45*, 87−90.

(13) Tao, X.; Li, J.; Möhwald, H. Self-assembly, optical behavior, and permeability of a novel capsule based on an azo dye and polyelectrolytes. *Chem. − Eur. J.* **2004**, *10* (14), 3397−3403.

(14) Dergunov, S. A.; Richter, A. G.; Kim, M. D.; Pingali, S. V.; Urban, V. S.; Pinkhassik, E. Synergistic self-assembly of scaffolds and building blocks for directed synthesis of organic nanomaterials. *Chem. Commun.* **2013**, *49* (94), 11026−11028.

(15) Bou, S.; Klymchenko, A. S.; Collot, M. Fluorescent labeling of biocompatible block copolymers: synthetic strategies and applications in bioimaging. *Mater. Adv.* **2021**, *2* (10), 3213−3233.

(16) Zheng, Y.; Yu, Z.; Parker, R. M.; Wu, Y.; Abell, C.; Scherman, O. A. Interfacial assembly of dendritic microcapsules with host-guest chemistry. *Nat. Commun.* **2014**, *5*, No. 5772.

(17) Amstad, E. Capsules: their past and opportunities for their future. *ACS Macro Lett.* **2017**, *6* (8), 841−847.

(18) Lima, A. L.; Gratieri, T.; Cunha-Filho, M.; Gelfuso, G. M. Polymeric nanocapsules: A review on design and production methods for pharmaceutical purpose. *Methods* **2022**, *199*, 54−66.

(19) Maor, I.; Koifman, N.; Kesselman, E.; Matsanov, P.; Shumilin, I.; Harries, D.; Weitz, I. S. Molecular self-assembly under nanoconfinement: indigo carmine scroll structures entrapped within polymeric capsules. *Nanoscale* **2021**, *13* (48), 20462−20470.

(20) Ding, S.; Serra, C. A.; Vandamme, T. F.; Yu, W.; Anton, N. Double emulsions prepared by two−step emulsification: History, state-of-the-art and perspective. *J. Controlled Release* **2019**, *295*, 31−49.

(21) Ristea, M.-E.; Zarnescu, O. Indigo carmine: between necessity and concern. *J. Xenobiot.* **2023**, *13* (3), 509−528.

(22) Sugimoto, M.; Koyama, Y.; Itoi, T.; Kawai, T. Using texture and colour enhancement imaging to evaluate gastrointestinal diseases in clinical practice: a review. *Ann. Med.* **2022**, *54* (1), 3314−3331.

(23) Monson, F. C.; Wein, A. J.; McKenna, B. A.; Whitmore, K.; Levin, R. M. Indigocarmine as a quantitative indicator of urothelial integrity. *J. Urol.* **1991**, *145* (4), 842−845.

(24) Kim, B. S.; Yoon, J. S.; Lim, S. A.; Han, Y. S.; Eo, S. R. Intraoperative injection of coloring dye in the surgical treatment of

https://doi.org/10.1021/acsomega.3c10447
ACS Omega 2024, 9, 13382−13390

hidradenitis suppurativa: A case report. *J. Wound Manage. Res.* **2022**, *18* (1), 48−52.
(25) Farah, S.; Anderson, D. G.; Langer, R. Physical and mechanical properties of PLA, and their functions in widespread applications — A comprehensive review. *Adv. Drug Delivery Rev.* **2016**, *107*, 367−392.
(26) Zhao, X.; Hu, H.; Wang, X.; Yu, X.; Zhou, W.; Peng, S. Super tough poly(lactic acid) blends: A comprehensive review. *RSC Adv.* **2020**, *10* (22), 13316−13368.
(27) Nofar, M.; Sacligil, D.; Carreau, P. J.; Kamal, M. R.; Heuzey, M.-C. Poly (lactic acid) blends: Processing, properties and applications. *Int. J. Biol. Macromol.* **2019**, *125*, 307−360.
(28) Saini, P.; Arora, M.; Kumar, M. N. V. R. Poly(lactic acid) blends in biomedical applications. *Adv. Drug Delivery Rev.* **2016**, *107*, 47−59.
(29) Riley, T.; Heald, C. R.; Stolnik, S.; Garnett, M. C.; Illum, L.; Davis, S. S.; King, S. M.; Heenan, R. K.; Purkiss, S. C.; Barlow, R. J.; et al. Core−shell structure of PLA−PEG nanoparticles used for drug delivery. *Langmuir* **2003**, *19* (20), 8428−8435.
(30) Rabanel, J.-M.; Hildgen, P.; Banquy, X. Assessment of PEG on polymeric particles surface, a key step in drug carrier translation. *J. Controlled Release* **2014**, *185*, 71−87.
(31) de Oliveira, M. A.; Araújo, R. S.; Mosqueira, V. C. F. PEGylated and functionalized polylactide-based nanocapsules: An overview. *Int. J. Pharm.* **2023**, *636*, No. 122760.
(32) Liang, H.; Friedman, J. M.; Nacharaju, P. Fabrication of biodegradable PEG−PLA nanospheres for solubility, stabilization, and delivery of curcumin. *Artif. Cells, Nanomed., Biotechnol.* **2017**, *45* (2), 297−304.
(33) Martino, C.; Lee, T. Y.; Kim, S.-H.; deMello, A. J. Microfluidic generation of PEG-b-PLA polymersomes containing alginate-based core hydrogel. *Biomicrofluidics* **2015**, *9* (2), No. 024101, DOI: 10.1063/1.4914112.
(34) Cho, H.; Gao, J.; Kwon, G. S. PEG-b-PLA micelles and PLGA-b-PEG-b-PLGA sol−gels for drug delivery. *J. Controlled Release* **2016**, *240*, 191−201.
(35) Feng, K.; Wei, Y.-S.; Hu, T.-G.; Linhardt, R. J.; Zong, M.-H.; Wu, H. Colon-targeted delivery systems for nutraceuticals: A review of current vehicles, evaluation methods and future prospects. *Trends Food Sci. Technol.* **2020**, *102*, 203−222.
(36) Thakral, S.; Thakral, N. K.; Majumdar, D. K. Eudragit: a technology evaluation. *Expert Opin. Drug Delivery* **2013**, *10* (1), 131−149.
(37) Patra, C. N.; Priya, R.; Swain, S.; Kumar Jena, G.; Panigrahi, K. C.; Ghose, D. Pharmaceutical significance of Eudragit: A review. *Future J. Pharm. Sci.* **2017**, *3* (1), 33−45.
(38) Sionkowska, A. Current research on the blends of natural and synthetic polymers as new biomaterials: Review. *Prog. Polym. Sci.* **2011**, *36* (9), 1254−1276.
(39) Joseph, J.; Parameswaran, R.; Panicker, U. G. Recent advancements in blended and reinforced polymeric systems as bioscaffolds. *Int. J. Polym. Mater. Polym. Biomater.* **2023**, *72* (11), 834−855.
(40) Coelho, M. G.; de Lima, G. M.; Augusti, R.; Maria, D. A.; Ardisson, J. D. New materials for photocatalytic degradation of Indigo Carmine—Synthesis, characterization and catalytic experiments of nanometric tin dioxide-based composites. *Appl. Catal., B* **2010**, *96* (1), 67−71.
(41) Mathematical models of drug release. In *Strategies to Modify the Drug Release from Pharmaceutical Systems*; Bruschi, M. L., Ed.; Woodhead Publishing, 2015; Chapter 5, pp 63−86.
(42) da Silva-Buzanello, R. A.; de Souza, M. F.; de Oliveira, D. A.; Bona, E.; Leimann, F. V.; Cardozo Filho, L.; de Araújo, P. H. H.; Ferreira, S. R. S.; Gonçalves, O. H. Preparation of curcumin-loaded nanoparticles and determination of the antioxidant potential of curcumin after encapsulation. *Polímeros* **2016**, *26*, 207−214.
(43) Gref, R.; Lück, M.; Quellec, P.; Marchand, M.; Dellacherie, E.; Harnisch, S.; Blunk, T.; Müller, R. H. 'Stealth' corona-core nanoparticles surface modified by polyethylene glycol (PEG): Influences of the corona (PEG chain length and surface density) and of the core composition on phagocytic uptake and plasma protein adsorption. *Colloids Surf., B* **2000**, *18* (3−4), 301−313.
(44) Asfour, M. H.; Mohsen, A. M. Formulation and evaluation of pH-sensitive rutin nanospheres against colon carcinoma using HCT-116 cell line. *J. Adv. Res.* **2018**, *9*, 17−26.
(45) Riley, T.; Govender, T.; Stolnik, S.; Xiong, C. D.; Garnett, M. C.; Illum, L.; Davis, S. S. Colloidal stability and drug incorporation aspects of micellar-like PLA−PEG nanoparticles. *Colloids Surf., B* **1999**, *16* (1), 147−159.
(46) Kister, G.; Cassanas, G.; Vert, M. Effects of morphology, conformation and configuration on the IR and Raman spectra of various poly(lactic acid)s. *Polymer* **1998**, *39* (2), 267−273.
(47) Riaz, U.; Ashraf, S. M. Characterization of polymer blends with FTIR spectroscopy. In *Characterization of Polymer Blends*; Wiley, 2014; pp 625−678.
(48) Martins, K. F.; Messias, A.; Leite, F.; Duek, E. Preparation and characterization of paclitaxel-loaded PLDLA microspheres. *Mater. Res.* **2014**, *17*, 650−656.
(49) Chollet, B.; Lopez-Cuesta, J.-M.; Laoutid, F.; Ferry, L. Lignin nanoparticles as a promising way for enhancing lignin flame retardant effect in polylactide. *Materials* **2019**, *12* (13), 2132.
(50) Mico-Vicent, B.; Martínez-Verdú, F. M.; Novikov, A.; Stavitskaya, A.; Vinokurov, V.; Rozhina, E.; Fakhrullin, R.; Yendluri, R.; Lvov, Y. Stabilized dye−pigment formulations with platy and tubular nanoclays. *Adv. Funct. Mater.* **2018**, *28* (27), No. 1703553.
(51) Costa, A. L.; Gomes, A. C.; Pillinger, M.; Gonçalves, I. S.; de Melo, J. S. S. An indigo carmine-based hybridnanocomposite with supramolecular control of dye aggregation and photobehavior. *Chem. − Eur. J.* **2015**, *21* (34), 12069−12078.
(52) Lyu, S.-P.; Sparer, R.; Hobot, C.; Dang, K. Adjusting drug diffusivity using miscible polymer blends. *J. Controlled Release* **2005**, *102* (3), 679−687.
(53) Gorrasi, G.; Pantani, R. Hydrolysis and biodegradation of poly(lactic acid). In *Synthesis, Structure and Properties of Poly(lactic acid)*; Di Lorenzo, M. L.; Androsch, R., Eds.; Springer International Publishing, 2018; pp 119−151.
(54) Aso, Y.; Yoshioka, S.; Li Wan Po, A.; Terao, T. Effect of temperature on mechanisms of drug release and matrix degradation of poly(D,L-lactide) microspheres. *J. Controlled Release* **1994**, *31* (1), 33−39.
(55) Turanlı, Y.; Acartürk, F. Preparation and characterization of colon-targeted pH/Time-dependent nanoparticles using anionic and cationic polymethacrylate polymers. *Eur. J. Pharm. Sci.* **2022**, *171*, No. 106122.
(56) Zhang, T.; Sturgis, T. F.; Youan, B.-B. C. pH-responsive nanoparticles releasing tenofovir intended for the prevention of HIV transmission. *Eur. J. Pharm. Biopharm.* **2011**, *79* (3), 526−536.
(57) Elsawy, M. A.; Kim, K.-H.; Park, J.-W.; Deep, A. Hydrolytic degradation of polylactic acid (PLA) and its composites. *Renewable Sustainable Energy Rev.* **2017**, *79*, 1346−1352.

https://doi.org/10.1021/acsomega.3c10447
ACS Omega 2024, 9, 13382−13390